Polyhedron 149 (2018) 39–44

Contents lists available at ScienceDirect

Polyhedron

journal homepage: www.elsevier.com/locate/poly

New insights in Mn–Ca chemistry from the use of oximate-based ligands: $\{Mn_{22}^{II/III}Ca_2\}$ and $\{Mn_2^{IV}Ca_2\}$ complexes with relevance to both low- and high-valent states of the oxygen-evolving complex

Alysha A. Alaimo [a], Dimitris I. Alexandropoulos [a], Christos Lampropoulos [b], Theocharis C. Stamatatos [a,*]

[a] Department of Chemistry, Brock University, 1812 Sir Isaac Brock Way, L2S 3A1 St. Catharines, Ontario, Canada
[b] Department of Chemistry, University of North Florida, 1 UNF Dr., Jacksonville, FL 32224, USA

ARTICLE INFO

Article history:
Received 8 February 2018
Accepted 17 April 2018
Available online 25 April 2018

Dedicated to Professor Spyros P. Perlepes on the occasion of his 65th birthday, and his contributions to coordination chemistry and molecular magnetism communities.

Keywords:
Mn–Ca complexes
Crystal structures
Oximato-based ligands
Oxygen-evolving complex
Magnetism

ABSTRACT

The initial use of quinoline-2-aldoxime (qaoH) and 2,6-diacetylpyridine dioxime ($dapdoH_2$) in heterometallic Mn–Ca chemistry has afforded a mixed-valence $\{Mn_{22}^{II/III}Ca_2\}$ cluster containing several $\{Mn_4CaO_x\}$ subunits and a 'butterfly'-like $\{Mn_2^{IV}Ca_2\}$ complex, respectively. The one-pot reaction of Mn $(O_2CPh)_2{\cdot}2H_2O$ and $Ca(O_2CPh)_2{\cdot}H_2O$ with qaoH and NEt_3 in a 1:1:1:1 molar ratio in a solvent mixture comprising MeCN/MeOH gave complex $[Mn_{22}Ca_2O_{14}(OH)_4(OMe)_6(O_2CPh)_{22}(qao)_2(MeCN)_2(H_2O)_4](OH)_2$ (**1**; $6Mn^{II}/16Mn^{III}$) in 20% yield. A similar reaction with that of **1**, albeit with $Mn(O_2CPh)_2{\cdot}2H_2O$ and $Ca(NO_3)_2{\cdot}4H_2O$ in the presence of $dapdoH_2$ and NEt_3, in a molar ratio of 1:1:2:2 in MeCN/MeOH, led to the smaller nuclearity complex $[Mn_2Ca_2(OMe)_2(NO_3)_2(dapdo)_4]$ (**2**; $2Mn^{IV}$) in 40% yield. The reported compounds demonstrate structural and magnetic relevance to both low- and high-valent states of the OEC.

1. Introduction

The burgeoning development of polynuclear metal cluster chemistry in recent years was spearheaded by the intense investigation of novel organic and/or inorganic bridging and chelating ligands [1,2]. Ligands with N- and/or O-donor atoms have also contributed to the emergence of many diverse physicochemical properties of cluster compounds. In the molecular magnetism arena, for instance, the ligands were found to significantly affect the nature of the magnetic exchange interactions between the metal ions [3], the orientation of magnetic anisotropy axes [4], and subsequently the magnetization dynamics of the molecular compounds [5]. Furthermore, different classes of organic bridging/chelating ligands have been employed as: (i) antennas for energy transfer purposes in the field of optics [6], (ii) spectators and actors in catalysis [7], and (iii) contrast agents in magnetic resonance imaging [8].

Bioinorganic chemistry is a thriving field of research and the impact of the ligands on the biocatalytic and biomimetic properties of polynuclear metal complexes has been manifested by the specific arrangement of the metal ions within the active site of Photosystem II (PSII) [9]. PSII is a multicomponent assembly of proteins and cofactors [10] that absorbs four photons to sequentially oxidize a $\{Mn_4CaO_5\}$ cluster compound (Scheme 1), known as the water-oxidizing complex (WOC) or the oxygen-evolving complex (OEC), through a four-electron process, namely the Kok cycle [11]. The latter involves a sequence of four S_n Kok states ($n = 0$ to 4). The most oxidized state of the Kok cycle is S_4, which participates in the O_2 release, while the S_1 is dubbed as the dark-adapted or dark-stable state [11,12]. The OEC consists of an oxido-bridged $\{Mn_3CaO_4\}$ distorted cubane unit linked to a fourth, dangling Mn atom through one of the unit's oxido bridges and an additional bis-μ-O^{2-} group (O5; Scheme 1) [13]. The inorganic core of the native catalytic site is surrounded by bridging amino acid residues and terminally ligated H_2O molecules or water-derived ligands (W1–W4; Scheme S1). This ligand organization within the OEC prompted scientists to attempt bench-top synthesis of structural analogues with similar -if not the same- geometrical, electronic and eventually catalytic properties [14]. Such synthetic endeavors pose several challenges, including (i) the formation of an oxido-bridged $\{Mn_4Ca\}$ core with an extended cubane structure, (ii) the stabilization of Mn ions in high oxidation states, and (iii)

* Corresponding author.
E-mail address: tstamatatos@brocku.ca (T.C. Stamatatos).

https://doi.org/10.1016/j.poly.2018.04.020
0277-5387/

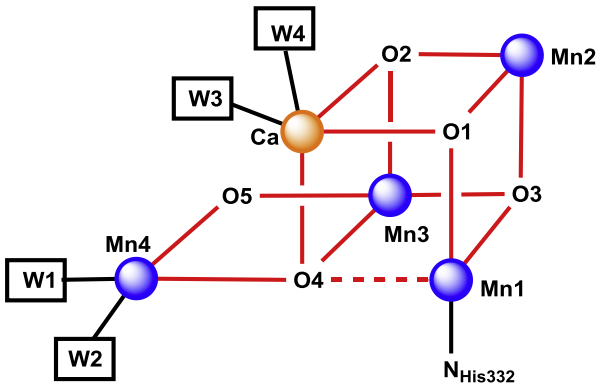

Scheme 1. Latest model for the {Mn_4CaO_5} inorganic core of the native OEC in PSII.

the choice of a ligand framework that would ideally support stability of the inorganic core in solution and access to multiple oxidation states.

Thus, the quest for new organic chelating/bridging ligands for heterometallic Mn–Ca chemistry is ongoing, with efforts focused on the incorporation of ligand moieties satisfying the aforementioned requirements. Simple carboxylates, hydroxamic acids, and polyalcohol-based ligands have been used in the synthesis of Mn–Ca complexes, leading to species with diverse topologies, oxidation state descriptions, and spectroscopic/physicochemical properties [14]. Oximes and dioximes have been extensively used in homometallic Mn cluster chemistry geared toward magnetism applications [15]; however, this class of ligands has no precedence in the Mn–Ca literature of biomimetic species. These ligands exhibit some interesting structural and electronic properties, among of which are their ability to (i) stabilize Mn ions in high oxidation states [16], (ii) support the formation and crystallization of Mn–O^{2-} inorganic cores [17], and (iii) potentially coordinate to oxophilic metal ions, such as Ca^{II}, due to the strong α-nucleophilic character of the oximate functionality. In addition, oximes are photosynthetically effective ligands and, in conjunction with hydrazine and nitric oxide, can reduce the OEC to S_{-1}, S_{-2} and S_{-3} states [18].

We herein report the initial employment of quinoline-2-aldoxime (qaoH) and 2,6-diacetylpyridine dioxime ($dapdoH_2$) in heterometallic Mn–Ca chemistry (Scheme 2), which has afforded the complexes $[Mn^{II}_6Mn^{III}_{16}Ca_2O_{14}(OH)_4(OMe)_6(O_2CPh)_{22}(qao)_2(MeCN)_2(H_2O)_4](OH)_2$ (**1**) and $[Mn^{IV}_2Ca_2(OMe)_2(NO_3)_2(dapdo)_4]$ (**2**), respectively. Complex **1** is the highest in nuclearity Mn–Ca cluster reported to date [19] and, although too high in nuclearity to model the exact structure of the native OEC, the presence of cubane-containing subunits within its structure render it a promising foundation for the low-valent species of OEC. Complex **2** is the first of its metal stoichiometry (Mn:Ca = 2:2) to have the Mn^{IV} ions in such a high oxidation state and therefore it can be related to one of the high-valent S_3 or S_4 states of the Kok cycle [11,12].

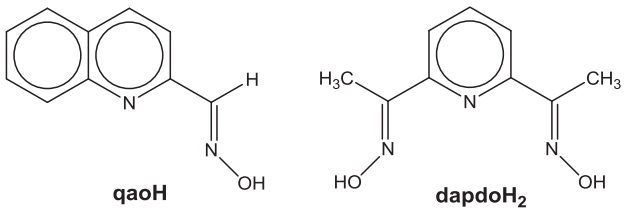

Scheme 2. Structural formulae and abbreviations of the oxime ligands used in this study.

2. Experimental

2.1. Materials and general methods

All manipulations were performed under aerobic conditions using chemicals and solvents as received, unless otherwise stated. The organic ligands qaoH and $dapdoH_2$ were prepared as described elsewhere [20]. The starting materials $Mn(O_2CPh)_2{\cdot}2H_2O$ and $Ca(O_2CPh)_2{\cdot}H_2O$ were synthesized in quantitative yields (>95%) from the reaction between $MnCl_2{\cdot}4H_2O$ or $CaCl_2{\cdot}2H_2O$ and excess of $PhCO_2H$ in $MeOH/H_2O$ (1:1 v/v) under basic conditions.

2.2. Preparation of complexes

2.2.1. $[Mn_{22}Ca_2O_{14}(OH)_4(OMe)_6(O_2CPh)_{22}(qao)_2(MeCN)_2(H_2O)_4](OH)_2$ (**1**)

To a stirred, yellow solution of qaoH (0.03 g, 0.2 mmol) and NEt_3 (28 μL, 0.2 mmol) in MeCN/MeOH (15:3 mL) the solids $Mn(O_2CPh)_2{\cdot}2H_2O$ (0.07 g, 0.2 mmol) and $Ca(O_2CPh)_2{\cdot}H_2O$ (0.06 g, 0.2 mmol) were added together. The resulting dark orange suspension was stirred for 30 min, during which time all the solids dissolved, and the colour of the solution changed to brown. The solution was filtered, and a mixture of Et_2O/C_6H_{14} (10 mL, 1/1 v/v) diffused into the filtrate. After a month, dark red needle-like crystals of **1** appeared and were collected by filtration, washed with cold MeCN (2 × 3 mL) and Et_2O (2 × 3 mL), and dried in air; the yield was 20% (based on the total available Ca). The crystalline solid was analyzed as **1**·$4H_2O$. *Anal.* Calc.: C, 43.90; H, 3.40; N, 1.67%. Found: C, 43.75; H, 3.27; N, 1.81%. Selected IR data (cm^{-1}): 1594 (m), 1567 (m), 1534 (m), 1491 (w), 1447 (w), 1386 (vs), 1303 (w), 1173 (w), 1143 (w), 1067 (w), 1020 (m), 984 (w), 936 (w), 829 (w), 710 (vs), 686 (m), 675 (m), 634 (w), 600 (m), 568 (m), 476 (w), 450 (w).

2.2.2. $[Mn_2Ca_2(OMe)_2(NO_3)_2(dapdo)_4]$ (**2**)

To a stirred, colourless solution of $dapdoH_2$ (0.08 g, 0.4 mmol) and NEt_3 (56 μL, 0.4 mmol) in MeCN/MeOH (15:5 mL) the solids $Mn(O_2CPh)_2{\cdot}2H_2O$ (0.07 g, 0.2 mmol) and $Ca(NO_3)_2{\cdot}4H_2O$ (0.05 g, 0.2 mmol) were added together. The resulting ecru suspension was stirred for 2 h, during which time all the solids dissolved, and the colour of the solution changed to dark brown. The solution was filtered and left to evaporate slowly at room temperature. After one week, dark brown rod-like crystals of **2**·2MeCN appeared and were collected by filtration, washed with cold MeCN (2 × 3 mL) and Et_2O (2 × 3 mL), and dried in air; the yield was 40% (based on the total available Ca). The crystalline solid was analyzed as lattice solvent-free **2**. *Anal.* Calc.: C, 40.01; H, 3.71; N, 17.19%. Found: C, 40.22; H, 3.78; N, 17.12%. Selected IR data (cm^{-1}): 2808 (w), 1591 (m), 1533 (m), 1409 (m), 1365 (w), 1316 (m), 1278 (w), 1190 (w), 1167 (m), 1149 (m), 1118 (w), 1087 (m), 1065 (m), 1015 (s), 947 (m), 822 (w), 805 (s), 792 (m), 760 (m), 684 (m), 663 (s), 553 (vs), 478 (m), 440 (m).

2.3. Physical measurements

Infrared (IR) spectra were recorded in the solid state on a Bruker's FT-IR spectrometer (ALPHA's Platinum ATR single reflection) in the 4000–400 cm^{-1} range. Elemental analyses (C, H, and N) were performed on a Perkin-Elmer 2400 Series II Analyzer. Magnetic susceptibility studies were performed in-house on a Quantum Design MPMS-XL SQUID susceptometer equipped with a 7 T magnet and operating in the 1.8–400 K range. Samples were embedded in solid eicosane to prevent torquing. Pascal's constants were used to estimate the diamagnetic correction, which was subtracted from the experimental susceptibility to give the molar paramagnetic susceptibility (χ_M) [21].

2.4. Single-crystal X-ray crystallography

Crystals of the complexes **1** and **2** were selected and mounted on MiteGen dual thickness micromounts TM using inert oil [22]. Diffraction data were collected at 100(2) K on a Bruker D8 VENTURE diffractometer equipped with a multilayer mirror monochromator and a Mo Kα microfocus sealed tube (λ = 0.71073 Å). Images were processed with the software SAINT+ [23], and absorption effects were corrected with the multi-scan method implemented in SADABS [24]. The structures were solved using the Bruker SHELXTL inside the APEX-III software package, and refined using the SHELXLE and PLATON programs [25]. The programs used for molecular graphics were MERCURY [26] and DIAMOND [27].

Additional information on the crystallographic data collection and structure refinement details is summarized in Table 1.

3. Results and discussion

3.1. Synthetic comments

The synthetic route followed for the synthesis of both **1** and **2** was based on the use of simple metal salts (i.e., metal carboxylates and nitrates) in conjunction with the desired chelating/bridging organic ligand (i.e., qaoH or dapdoH_2) and an external base (i.e., NEt_3) to facilitate the deprotonation of the employed chelates. Therefore, the one-pot reaction of $Mn(O_2CPh)_2{\cdot}2H_2O$ and $Ca(O_2CPh)_2{\cdot}H_2O$ with qaoH and NEt_3 in a 1:1:1:1 M ratio in a solvent mixture comprising MeCN/MeOH gave a brown solution that, upon filtration and layering with Et_2O/hexanes, afforded dark red needle-like crystals of the mixed-valence complex $[Mn_{22}Ca_2O_{14}(OH)_4(OMe)_6(O_2CPh)_{22}(qao)_2(MeCN)_2(H_2O)_4](OH)_2$ (**1**; $6Mn^{II}/16Mn^{III}$) in 20% yield (based on the total available Ca). A similar reaction with that of **1**, albeit with $Mn(O_2CPh)_2{\cdot}2H_2O$ and $Ca(NO_3)_2{\cdot}4H_2O$ in the presence of dapdoH_2 and NEt_3, in a molar ratio of 1:1:2:2 in MeCN/MeOH, led to a dark brown solution that, upon filtration and slow evaporation at room temperature, afforded dark-brown rod-like crystals of the new complex $[Mn_2Ca_2(OMe)_2(NO_3)_2(dapdo)_4]$ (**2**; $2Mn^{IV}$) in 40% yield (based on the total available Ca).

The reactions that gave **1** and **2** are both oxidations, undoubtedly by atmospheric O_2 under the prevailing basic conditions. Employment of different organic bases, such as NMe_3, $Bu^n{}_3N$ and Me_4NOH, did not afford crystalline materials but only oily products that we were not able to further characterize. It becomes apparent that the reaction solvent has an important role in the synthesis and crystallization of both **1** and **2**; bridging MeO^- groups and terminally-bound or lattice MeCN molecules were found in the structures of **1** and **2** (*vide infra*). Reactions in different alcohols did not yield any crystalline materials but only amorphous precipitates that we were unable to re-dissolve and crystallize. Analogous reactions with different carboxylate-based starting materials (i.e., acetates, propionates, pivalates, etc.), all failed to yield single-crystals suitable for X-ray diffraction studies. Finally, by adjusting the experimental molar ratios of the precursors to the stoichiometric equivalents, in an attempt to optimize the isolated yields, we failed to reproduce the crystals of both complexes **1** and **2**.

Table 1
Crystallographic data for complexes **1** and **2**.

Parameter	**1**	**2**
Formula	$C_{184}H_{162}Mn_{22}Ca_2N_6O_{76}$	$C_{38}H_{42}Mn_2Ca_2N_{14}O_{16}$
Fw (g mol^{-1})	4962.13	1140.88
Crystal type	dark red needle	dark brown rod
Crystal size (mm^3)	0.20 × 0.20 × 0.20	0.10 × 0.20 × 0.40
Crystal system	triclinic	monoclinic
Space group	$P\bar{1}$	$P2_1/n$
a (Å)	17.226(5)	13.5003(12)
b (Å)	18.581(4)	12.9259(12)
c (Å)	19.604(3)	15.2726(13)
α (°)	68.823(4)	90
β (°)	68.416(8)	104.320(3)
γ (°)	68.981(8)	90
V (Å^3)	5253.1(2)	2582.3(4)
Z	1	2
D_{calc} (g cm^{-3})	1.587	1.467
μ (mm^{-1})	1.407	0.765
θ (°)	2.24 to 25.99	2.21 to 26.02
Index ranges	$-21 \le h \le 21$	$-16 \le h \le 16$
	$-22 \le k \le 22$	$-15 \le k \le 15$
	$-24 \le l \le 24$	$-18 \le l \le 18$
Reflections collected	221412	39911
Independent reflections	20527 (R_{int} = 0.0644)	5072 (R_{int} = 0.0773)
Final R indices [$I > 2\sigma(I)$][a,b]	R_1 = 0.0531	R_1 = 0.0374
	wR_2 = 0.1456	wR_2 = 0.0871
Final R indices (all data)	R_1 = 0.0730	R_1 = 0.0596
	wR_2 = 0.1597	wR_2 = 0.0968
$(\Delta\rho)_{maximum,minimum}$ (e Å^{-3})	2.090 and −2.367	0.550 and −0.454

[a] $R_1 = \Sigma(||F_o| - |F_c||)/\Sigma|F_o|$.
[b] $wR_2 = [\Sigma[w(F_o^2 - F_c^2)^2]/\Sigma[w(F_o^2)^2]]^{1/2}$, $w = 1/[\sigma^2(F_o^2) + [(ap)^2 + bp]$, where $p = [\max(F_o^2, 0) + 2F_c^2]/3$.

3.2. Description of structures

The formulae of **1** and **2** are based on metric parameters, charge-balance considerations, and bond valence sum (BVS) calculations on the Mn and O atoms (ESI). The presence of OH^- counterions in **1** is not unusual in high-nuclearity metal cluster chemistry [28]. The molecular structure of the centrosymmetric cation of **1** (Fig. 1, top) consists of 6 Mn^{II}, 16 Mn^{III} and 2 Ca^{II} ions held together by 12 μ_4-O^{2-}, 2 μ_3-O^{2-}, 4 μ_3-OH^-, 4 μ_3-OMe^-, 2 μ-OMe^- and 2 μ_4-oximate groups from two $\eta^1{:}\eta^1{:}\eta^3{:}\mu_4$ qao$^-$ ligands (Scheme S1). Peripheral ligation about the $[Mn^{II}_6Mn^{III}_{16}Ca_2(\mu_4\text{-}O)_{12}(\mu_3\text{-}O)_2(\mu_3\text{-}OH)_4(\mu_3\text{-}OMe)_4(\mu\text{-}OMe)_2(\mu_4\text{-}NO)_2]^{22+}$ core (Fig. 1, bottom) is provided by 22 $PhCO_2^-$ groups that are either μ- or μ_3-bridging and terminally bound (Scheme S1), as well as two and four terminally coordinated MeCN and H_2O molecules located on the Ca1/Ca1′, Mn7/Mn7′ and Mn10/Mn10′ pairs, respectively. Four coordinated H_2O molecules are also present in the active site of the native OEC, two of which are bound to a Mn ion [13]. These H_2O molecules could serve as substrates for the overall catalytic reaction to proceed, including subsequent deprotonations with metal-centered oxidations preceding O-O bond formation [11–13].

The unique topology of **1** can be described as four $\{Mn^{II}Mn^{III}_3O_4\}$ cubanes that are connected to each other through a central $\{Mn_2O_4\}$ unit comprising the atoms Mn8, Mn8′, O7 and O7′. Each of the external cubane subunits is further linked to a $\{Mn^{II}Mn^{III}Ca(\mu_3\text{-}NO)\}$ unit through the bridging oxido, methoxido and oximate groups. As a result, within **1**, there are four symmetry-related $\{Mn_4O_4\}$ distorted cubanes attached to two "dangling" Ca^{II} atoms. The structures of these $\{Mn_4CaO_5\}$ and $\{Mn_4CaO_6\}$ subunits (Fig. 2) are intriguing, especially when compared to the OEC. In particular, they possess a similar extended cubane topology to that of the native site, with Mn···Mn and Mn···Ca closest separations of 2.876–3.686 Å and 3.376–3.756 Å, respectively, comparable to the corresponding values of 2.7–3.3 Å and ~3.4 Å for the OEC in PSII. All Mn atoms in **1** are six-coordinate with distorted octahedral geometries. In the case of the Mn^{III} atoms [Mn(2–9) and their symmetry-related partners], the octahedra are axially elongated due to the Jahn–Teller (JT) distortions, as expected for high-spin d^4 ions in this geometry. In addition, both Ca^{II} atoms in **1** are five-coordinate with an almost perfect square pyramidal geometry (τ = 0.05) [29]. Finally, the space-filling representation (Fig. S2) shows that **1** adopts a nano-sized ellipsoidal conformation with dimensions of ~26 and ~20 Å, defined by the longest C···C distances, excluding the H-atoms.

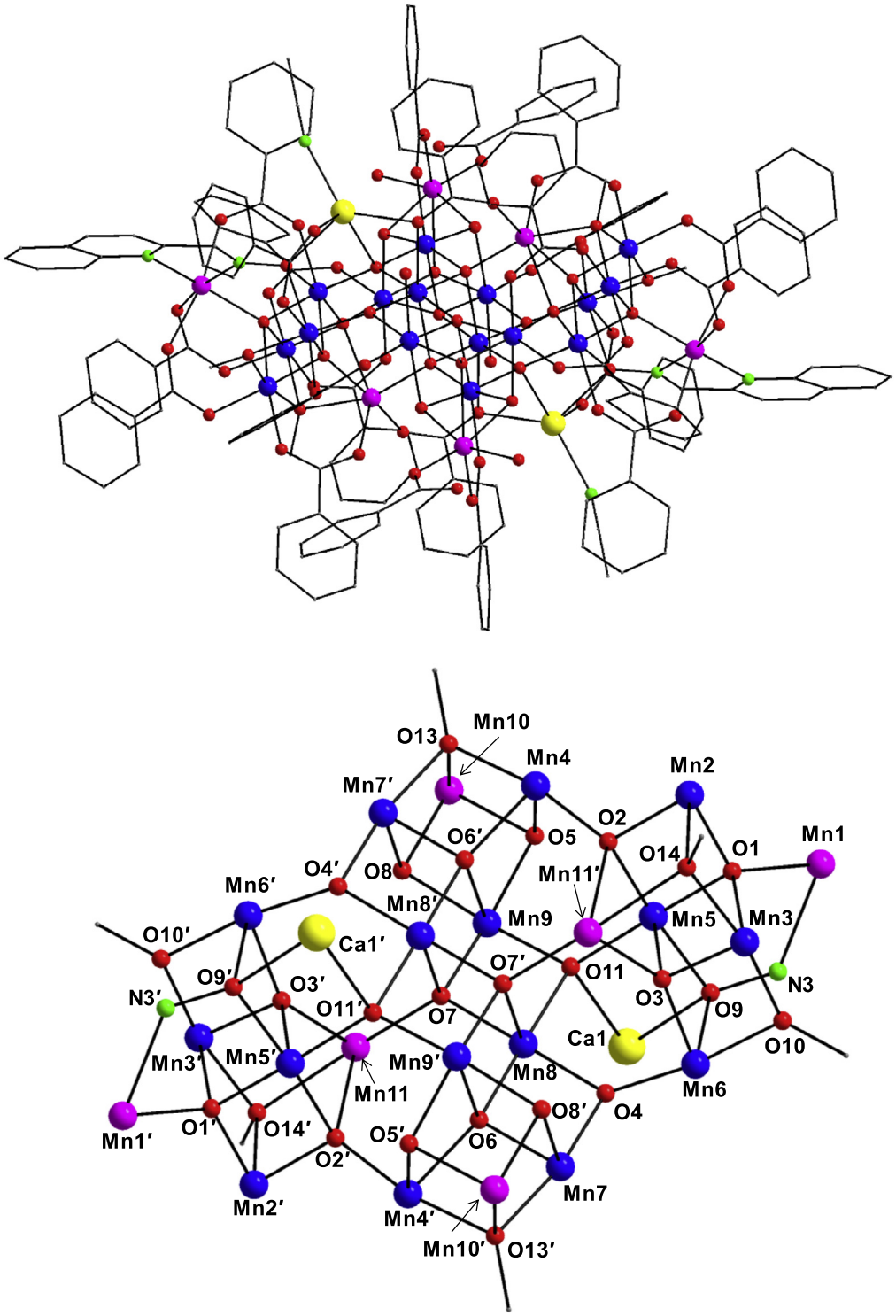

Fig. 1. Molecular structure of the cation of **1** (top) and a labelled representation of its complete core (bottom). Colour scheme: Mn^{II} purple, Mn^{III} blue, Ca^{II} yellow, O red, N green, C gray. H atoms are omitted for clarity. Symmetry operation for the primed atoms in **1**: 1−*x*, 1−*y*, 1−*z*. (Colour online.)

The structure of **2** (Fig. 3) contains an unusual 'butterfly'-like core where the high-valence Mn^{IV} ions are located at the wing-tip positions and the two Ca^{II} ions occupying the 'body' sites. The metal ions are bridged by two μ-OMe^- (O1, O1′) and the oximate arms of two $\eta^1{:}\eta^1{:}\eta^1{:}\eta^1{:}\eta^1{:}\mu_3$ and two $\eta^1{:}\eta^1{:}\eta^1{:}\eta^2{:}\mu_3$ $dapdo^{2-}$ ligands (Scheme S2). The dioximate ligands appear to both chelate and bridge the Mn^{IV} and Ca^{II} ions by employing all four of their donor atoms albeit under different configurations. This emphasizes the versatility, flexibility and ability of $dapdo^{2-}$ to stabilize metal ions in various oxidation states, diverse sizes and different intrinsic characteristics (hardness, acidity and oxophilicity). The six-coordinate Mn^{IV} ions possess distorted octahedral geometries, whereas two bidentate chelating NO_3^- groups complete eight-coordination around each Ca^{II} ion. The coordination geometry of both Ca^{II} ions is very distorted; the program SHAPE [30] was used to determine the CShM values of 3.71 and 3.88 for square antiprismatic and

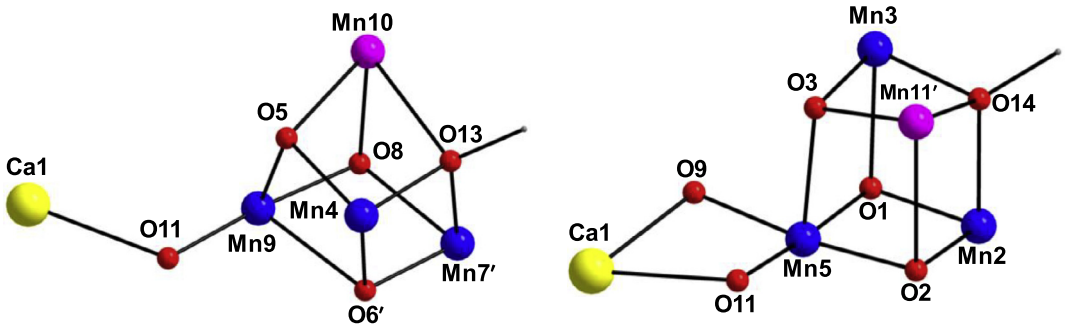

Fig. 2. Two types of {Mn_4Ca} extended cubane subunits found within **1**. Colour scheme as in Fig. 1. (Colour online.)

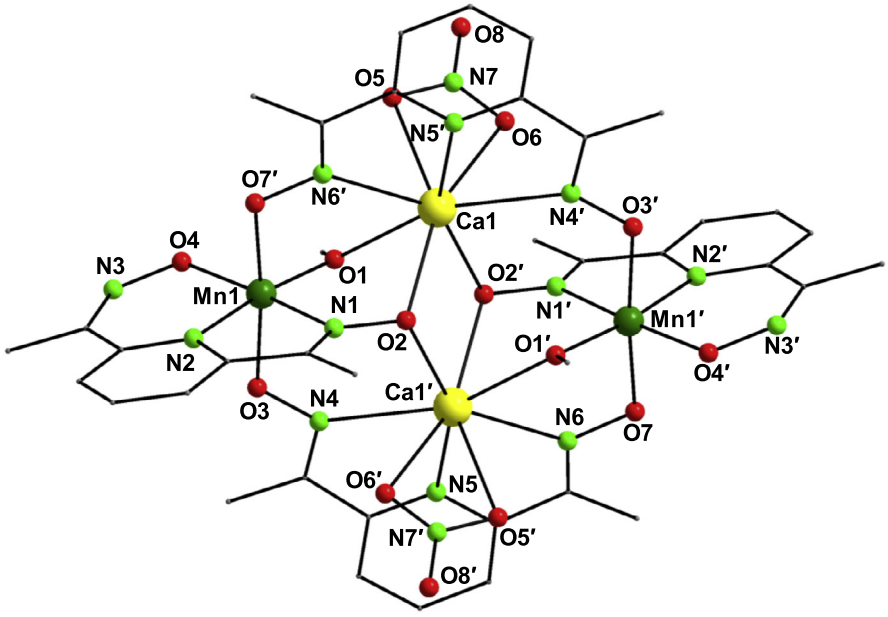

Fig. 3. Labelled structure of **2**. Colour scheme: Mn^{IV} olive green, Ca^{II} yellow, O red, N green, C gray. H atoms are omitted for clarity. Symmetry operation for the primed atoms in **2**: 1−*x*, 1−*y*, 1−*z*. (Colour online.)

triangular dodecahedral geometries, respectively (Fig. S3, ESI). The Mn···Mn and Mn···Ca distances are 6.717 Å and 3.561/4.067 Å, respectively. Complex **2** is the first non-oxido bridged Mn–Ca complex that contains exclusively Mn^{IV} ions; this is clearly supported by the oximate arms of $dapdo^{2-}$ ligands.

Complexes **1** and **2** do not appear to retain their solid-state structures in solutions of various solvent media (i.e., MeCN, CH_2Cl_2, and THF), as it was confirmed by electrospray ionization mass spectrometry. We have instead focused on the solid-state characterization, which includes IR spectroscopy (ESI) and magnetic studies.

3.3. Magnetic susceptibility studies

Variable-temperature direct-current (*dc*) magnetic susceptibility measurements were performed on freshly-prepared and analytically-pure microcrystalline samples of **1** and **2** in the temperature range 2–300 K in an applied field of 0.1 T. The data are shown as $\chi_M T$ *vs.* *T* plots in Fig. 4. The value of the $\chi_M T$ product for **1** at 300 K is 41.74 $cm^3 \cdot mol^{-1} \cdot K$, significantly lower than the value of 74.25 $cm^3 \cdot mol^{-1} \cdot K$ (calculated with $g = 2$) expected for 6 Mn^{II} and 16 Mn^{III} non-interacting ions. The $\chi_M T$ of **1** steadily decreases with decreasing *T*, reaching a value of 1.56 $cm^3 \cdot mol^{-1} \cdot K$ at 2 K. The overall magnetic response of **1** is indicative of predominant antiferromagnetic exchange interactions between the metal centers, and the low $\chi_M T$ value at 2 K suggests a very small spin ground state value. The latter was confirmed to be $S = 0$ by extrapolation of the $\chi'_M T$ *ac* data down to 0 K (Fig. S4). The $\chi'_M T$ is heading to a

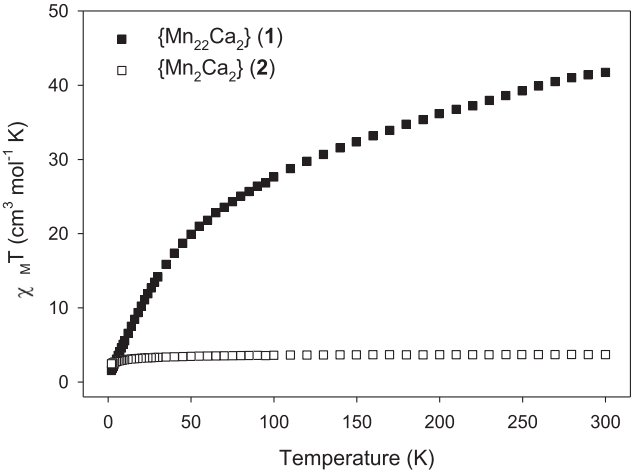

Fig. 4. $\chi_M T$ *vs.* *T* plots for **1** and **2** in a 1 kG field.

value of ~0 $cm^3 \cdot mol^{-1} \cdot K$, in agreement with an $S = 0$ ground state. The structure of **1** is too complicated to allow for any accurate and precise rationalization of the $S = 0$. Although discrete $\{Mn_4O_4\}$ cubanes at various oxidation state descriptions are generally known to be ferromagnetically coupled for a wide range of Mn–O–Mn angles [31], such cubane subunits in **1** are linked to each other *via* oxido groups, one of the strongest antiferromagnetic couplers in molecular magnetism. The Mn^{IV} ions in complex **2** are well separated from each other and there is very weak to negligible magnetic interaction between them, as indicated by the temperature independence of the $\chi_M T$ product from 300 to 5 K. The $\chi_M T$ of **2** remains essentially constant to a value of ~3.7 $cm^3 \cdot mol^{-1} \cdot K$, very close to the theoretical value of 3.75 $cm^3 \cdot mol^{-1} \cdot K$ (calculated with $g = 2$) for two non-interacting Mn^{IV} (d^3; $S = 3/2$) ions. The low-T decrease (<5 K) of the $\chi_M T$ could be tentatively ascribed to the onset of some weak magnetic coupling between the metal centres, of either intra- or intermolecular origin, zero-field splitting and/or Zeeman effects from the applied *dc* field.

4. Conclusions and perspectives

In conclusion, we have shown that oximate and dioximate chelating/bridging ligands can support the formation and crystallization of structurally new Mn–Ca complexes with diverse nuclearities, topologies, metal stoichiometries and oxidation state descriptions. Complexes **1** and **2** join a growing, but still small, list of structurally characterized Mn–Ca complexes [14,19,32], thus emphasizing the continuous need for the development of new ligand systems and synthetic routes for the isolation of new structural models of the OEC. Although the overall structures of the reported compounds are strictly not similar to that of the native OEC, we nevertheless believe that this work provides a foundation from which to tackle the synthesis of the discrete $\{Mn_4Ca\}$ unit responsible for the O_2 gas evolution. This could be accomplished by modifying the reaction conditions that yielded **1** to foster lower nuclearity products, hopefully with the correct topology and metal stoichiometry as those of the OEC. The incorporation of bridging oxido groups in **2** could also facilitate the formation of Mn^{IV}–Ca/O^{2-} complexes with dioximate ligands. Both the described strategies, and others, are currently under investigation.

Acknowledgements

This work was supported by the NSERC-DG, ERA and Brock University (to Th.C.S), the Research Corp. (to C.L), and the National Science Foundation (grants DMR-1429428/DMR-1626332 to C.L).

Appendix A. Supplementary data

CCDC 1588820, 1588821 contains the supplementary crystallographic data for (**1**) and (**2**). These data can be obtained free of charge via http://www.ccdc.cam.ac.uk/conts/retrieving.html, or from the Cambridge Crystallographic Data Centre, 12 Union Road, Cambridge CB2 1EZ, UK; fax: (+44) 1223-336-033; or e-mail: deposit@ccdc.cam.ac.uk. Supplementary data associated with this article can be found, in the online version, at https://doi.org/10.1016/j.poly.2018.04.020.

References

[1] For a recent review, see: C. Papatriantafyllopoulou, E.E. Moushi, G. Christou, A. J. Tasiopoulos Chem. Soc. Rev. 45 (2016) 1597.
[2] (a) A.J. Tasiopoulos, S.P. Perlepes, Dalton Trans. (2008) 5537;
(b) G. Aromi, E.K. Brechin, Struct. Bond. 122 (2006) 1;
(c) R.E.P. Winpenny, J. Chem. Soc., Dalton Trans. (2002) 1.
[3] (a) O. Kahn, Molecular Magnetism, VCH Publishers, New York, 1993;
(b) C. Benelli, D. Gatteschi, Chem. Rev. 102 (2002) 2369.
[4] J.D. Rinehart, J.R. Long, Chem. Sci. 2 (2011) 2078.
[5] R. Layfield, M. Murugesu, Lanthanides and Actinides in Molecular Magnetism, John-Wiley & Sons, 2015.
[6] J.-C.G. Bünzli, S.V. Eliseeva, Chem. Sci. (2013) 1939.
[7] M. Stradiotto, R.J. Lundgren (Eds.), Ligand Design in Metal Chemistry: Reactivity and Catalysis, Wiley, 2016.
[8] W. Krausse (Ed.), Contrast Agents 1: Magnetic Resonance Imaging – Topics in Current Chemistry, Springer, 2002.
[9] J.P. McEvoy, G.W. Brudvig, Chem. Rev. 106 (2006) 4455.
[10] Y. Umena, K. Kawakami, J.-R. Shen, N. Kamiya, Nature 473 (2011) 55.
[11] (a) J. Yano, V. Yachandra, Chem. Rev. 114 (2014) 4175;
(b) S. Paul, F. Neese, D.A. Pantazis, Green Chem. 19 (2017) 2309.
[12] (a) B. Kok, B. Forbush, M. McGloin, Photochem. Photobiol. 11 (1970) 457;
(b) D.R.J. Kolling, N. Cox, G.M. Ananyev, R.J. Pace, G.C. Dismukes, Biophys. J. 103 (2012) 313.
[13] (a) J. Yano, J. Kern, K. Sauer, M.J. Latimer, Y. Pushkar, J. Biesiadka, B. Loll, W. Saenger, J. Messinger, A. Zouni, V.K. Yachandra, Science 314 (2006) 821;
(b) J. Barber, Biochemistry 55 (2016) 5901;
(c) D.A. Pantazis, W. Ames, N. Cox, W. Lubitz, F. Neese, Angew. Chem., Int. Ed. 51 (2012) 9935.
[14] (a) S. Mukherjee, J.A. Stull, J. Yano, ThC. Stamatatos, K. Pringouri, T.A. Stich, K. A. Abboud, R.D. Britt, V.K. Yachandra, G. Christou, Proc. Natl. Acad. Sci. 109 (2012) 2257;
(b) E.S. Koumousi, S. Mukherjee, C.M. Beavers, S.J. Teat, G. Christou, ThC. Stamatatos, Chem. Commun. 47 (2011) 11128;
(c) B. Gerey, E. Gouré, J. Fortage, J. Pécaut, M.-N. Collomb, Coord. Chem. Rev. 319 (2016) 1;
(d) C. Zhang, C. Chen, H. Dong, J.-R. Shen, H. Dau, J.A. Zhao, Science 348 (2015) 690;
(e) J.S. Kanady, E.Y. Tsui, M.W. Day, T.A. Agapie, Science 333 (2011) 733.
[15] (a) Th.C. Stamatatos, D. Foguet-Albiol, S.-C. Lee, C.C. Stoumpos, C.P. Raptopoulou, A. Terzis, W. Wernsdorfer, S.O. Hill, S.P. Perlepes, G. Christou, J. Am. Chem. Soc. 129 (2007) 9484;
(b) C.J. Milios, A. Vinslava, W. Wernsdorfer, S. Moggach, S. Parsons, S.P. Perlepes, G. Christou, E.K. Brechin, J. Am. Chem. Soc. 129 (2007) 2754;
(c) T.N. Nguyen, W. Wernsdorfer, M. Shiddiq, K.A. Abboud, S. Hill, G. Christou, Chem. Sci. 7 (2016) 1156.
[16] (a) C.J. Milios, Th.C. Stamatatos, S.P. Perlepes, Polyhedron 25 (2006) 134;
(b) C.J. Milios, S. Piligkos, E.K. Brechin, Dalton Trans. (2008) 1809.
[17] (a) D.I. Alexandropoulos, C. Papatriantafyllopoulou, G. Aromí, O. Roubeau, S.J. Teat, S.P. Perlepes, G. Christou, Th.C. Stamatatos, Inorg. Chem. 49 (2010) 3962;
(b) D.I. Alexandropoulos, C. Papatriantafyllopoulou, C. Li, L. Cunha-Silva, M.J. Manos, A.J. Tasiopoulos, W. Wernsdorfer, G. Christou, Th.C. Stamatatos, Eur. J. Inorg. Chem. (2013) 2286.
[18] (a) W.F. Beck, G.W. Brudvig, Biochemistry 26 (1987) 8285;
(b) P.J. Riggs-Gelasco, R. Mei, C.F. Yocum, J.E. Penner-Hahn, J. Am. Chem. Soc. 118 (1996) 2387.
[19] (a) N.E. Chakov, A.E. Thuijs, W. Wernsdorfer, A.L. Rheingold, K.A. Abboud, G. Christou, Inorg. Chem. 55 (2016) 8468;
(b) A. Mishra, W. Wernsdorfer, K.A. Abboud, G. Christou, Chem. Commun. (2005) 54.
[20] (a) E. Abele, R. Abele, K. Rubina, E. Lukevics, Chem. Heterocycl. Compd. 41 (2005) 137;
(b) C.W. Glynn, M.M. Turnbull, Trans. Met. Chem. 27 (2002) 822.
[21] G.A. Bain, J.F. Berry, J. Chem. Educ. 85 (2008) 532.
[22] https://www.mitegen.com/product/loops/.
[23] SAINT+, Data Integration Engine v. 8.27b©, Bruker AXS, Madison, Wisconsin, USA, 1997-2012.
[24] G.M. Sheldrick, SADABS 2012, 1, Bruker AXS Area Detector Scaling and Absorption Correction Program, Bruker AXS, Madison Wisconsin, USA, 2012.
[25] (a) APEX-III Bruker, AXS Inc., Madison, Wisconsin, USA, 2016.;
(b) C.B. Hübschle, G.M. Sheldrick, B. Dittrich, J. Appl. Cryst. 44 (2011) 1281;
(c) A.L. Spek, J. Appl. Cryst. 36 (2003) 7.
[26] I.J. Bruno, J.C. Cole, P.R. Edgington, M.K. Kessler, C.F. Macrae, P. McCabe, J. Pearson, R. Taylor, Acta Crystallogr., Sect. B 58 (2002) 389.
[27] K. Bradenburg, DIAMOND, Release 3.1f, Crystal Impact GbR; Bonn, Germany, 2008.
[28] (a) E. Moushi, C. Lampropoulos, W. Wernsdorfer, V. Nastopoulos, G. Christou, A.J. Tasiopoulos, J. Am. Chem. Soc. 132 (2010) 16146;
(b) D.I. Alexandropoulos, K.M. Poole, L. Cunha-Silva, J. Ahmad Sheikh, W. Wernsdorfer, G. Christou, Th.C. Stamatatos, Chem. Commun. 53 (2017) 4266.
[29] A.W. Addison, T.N. Rao, J. Reedijk, J. Rijn, G.C. Verschoor, J. Chem. Soc., Dalton Trans. (1984) 1349.
[30] S. Alvarez, P. Alemany, D. Casanova, J. Cirera, M. Llunell, D. Avnir, Coord. Chem. Rev. 249 (2005) 1693.
[31] O. Kahn, Magnetism: A Supramolecular Function, Springer 484 (1996) 1–660.
[32] (a) A.A. Alaimo, E.S. Koumousi, L. Cunha-Silva, L.J. McCormick, S.J. Teat, V. Psycharis, C.P. Raptopoulou, S. Mukherjee, C.R. Li, S. Das Gupta, A. Escuer, G. Christou, Th.C. Stamatatos, Inorg. Chem. 56 (2017) 10760–10774;
(b) S. Melnic, S. Shova, A.C. Benniston, P.G. Waddell, CrystEngComm 19 (2017) 3674;
(c) L. Escriche-Tur, J. Jover, M. Font-Bardia, G. Aullon, M. Corbella, Inorg. Chem. 54 (2015) 11596.